One potential application of these arrays is as field emitter arrays for vacuum microelectronic devices. The possibility that large arrays can be self-assembled using simple thin-film processes without the need for expensive lithography makes them interesting for the field emission display industry (*14*). Currently, metal field emitters are fabricated using an elaborate process [the Spindt process (*7*)] involving photolithographic definition of individual emitter wells and the subsequent deposition of the refractory metals to form the periodic arrays of emitters. An intrinsic feature of the Spindt process is the need to carry out expensive micrometer- or submicrometer-scale photolithography, which is not cost-effective for large-area displays. To explore the feasibility of field-assisted electron emission, we obtained PEEM images from these arrays under an applied field of 30 kV/cm and ultraviolet light of energy ~5 eV. Because the surface work function of PdO_2 is ~3.9 eV (*15*), the tips were expected to emit electrons under these conditions. The PEEM image (Fig. 4A) shows a distribution of bright spots with a typical spacing of about 1.5 to 2.5 μm, which is consistent with the spacing of the tips as measured from AFM images (Fig. 4B). The less bright spots are perhaps emission from the edges of the tips. Analysis of bright-field patterns in the PEEM images reveals the bright-field spot density to be $\sim 47 \times 10^6$ tips/cm^2. This result is consistent with the density of tips determined from the AFM images for the same sample, which we estimate (number of tips of average height and above) to be $\sim 46 \times 10^6$ tips/cm^2. This density of tips or field emitter cones is well within the specifications for current field emission displays, which require $\sim 6 \times 10^6$ tips/cm^2 (based on current density of 1 μA) for each subpixel (50 μm by 300 μm) for a 15-inch SVGA monitor (*14*). To further justify the use of these tips as field emission arrays, we have controlled the tip-to-tip distance, their aspect ratio, and the tip radius by controlling the thickness and grain size of the starting Pd film. Finally, these emitters can be gated using a scheme similar to that used for Si field emitter arrays (*5*).

References and Notes

1. F. M. d'Heurle, *Int. Mater. Rev.* **34**, 53 (1989) and references therein.
2. F. R. N. Nabarro, in *Report of a Conference on Strength of Solids* (The Physical Society, London, 1948), p. 75.
3. C. Herring, *J. Appl. Phys.* **21**, 437 (1950).
4. R. L. Coble, *J. Appl. Phys.* **34**, 1679 (1963).
5. D. Temple, *Mat. Sci. Eng.* **R24**, 185 (1999).
6. M. R. Rakhshandehroo, J. W. Weigold, W.-C. Tian, S. W. Pang, *J. Vac. Sci. Technol. B* **16**, 2849 (1998).
7. C. A. Spindt, *J. Appl. Phys.* **39**, 3504 (1968).
8. Q. Xie, A. Madhukar, P. Chen, N. P. Kobayashi, *Phys. Rev. Lett.* **75**, 2542 (1995).
9. V. A. Schhukin and D. Bimberg, *Rev. Mod. Phys.* **71**, 4 (1999), and references therein.
10. B. C. Chakoumakos, D. G. Schlom, M. Urbanik, J. Luine, *J. Appl. Phys.* **83**, 1979 (1998).
11. K.-H. Hellwege and A. M. Hellwege, Eds., *Landolt-Bornstein Numerical Data and Functional Relationships in Science and Technology* (Springer-Verlag, New York, 1975), vol. 7, p. 26.
12. L. Holborn and A. L. Day, *Ann. Phys.* **4**, 104 (1901).
13. I. M. Lifschitz and V. V. Slyozov, *Phys. Chem. Solids* **19**, 35 (1961).
14. B. R. Chalamala, Y. Wei, B. E. Gnade, *IEEE Spectrum* **35**, 42 (1998).
15. J. H. Bernhard, E. D. Sosa, D. E. Golden, B. R. Chalamala, Y. Wei, R. H. Reuss, S. Aggarwal, R. Ramesh, unpublished data.

16. Supported in part by NSF Materials Research Science and Engineering Center grant DMR96-32521 and Laboratory for Physical Sciences and by a University of Maryland Distinguished Research Faculty Fellowship (R.R.).

15 November 1999; accepted 4 February 2000

Generation of Femtosecond Pulses of Synchrotron Radiation

R. W. Schoenlein,[1]* S. Chattopadhyay,[2] H. H. W. Chong,[4] T. E. Glover,[3] P. A. Heimann,[3] C. V. Shank,[1] A. A. Zholents,[2] M. S. Zolotorev[2]

Femtosecond synchrotron pulses were generated directly from an electron storage ring. An ultrashort laser pulse was used to modulate the energy of electrons within a 100-femtosecond slice of the stored 30-picosecond electron bunch. The energy-modulated electrons were spatially separated from the long bunch and used to generate ~300-femtosecond synchrotron pulses at a bend-magnet beamline, with a spectral range from infrared to x-ray wavelengths. The same technique can be used to generate ~100-femtosecond x-ray pulses of substantially higher flux and brightness with an undulator. Such synchrotron-based femtosecond x-ray sources offer the possibility of applying x-ray techniques on an ultrafast time scale to investigate structural dynamics in condensed matter.

An important scientific frontier is the application of x-ray pulses to investigate ultrafast structural dynamics (atomic motion and rearrangement) associated with phase transitions in solids, chemical reactions, and rapid biological processes. The fundamental time scale for such motion is an atomic vibrational period, on the order of 100 fs. Such dynamics have been investigated to date primarily with visible pulses from mode-locked femtosecond lasers (*1*) that probe only extended electronic states providing indirect information about atomic structure. X-rays, on the other hand, interact with core electronic levels and can therefore provide direct information about atomic structure. Rapid advances in our understanding of condensed matter structure at the atomic scale have been driven by modern synchrotrons providing high-brightness x-ray beams (*2*). However, the time resolution available from synchrotrons is nearly three orders of magnitude too slow to probe atomic motion within a single vibrational period. Recent efforts at applying x-rays to probe structural dynamics have used a synchrotron source combined with a picosecond-resolution x-ray streak camera (*3*) or relatively low brightness subpicosecond x-ray sources based on laser-produced plasmas (*4, 5*), laser-driven diodes (*6*), and relativistic Thomson scattering (*7, 8*). We demonstrate the generation of femtosecond pulses at a synchrotron beamline using femtosecond laser pulses (*9*), which is a promising approach to extend the time resolution of high-brightness synchrotron x-ray sources to 100 fs and will enable the study of structural dynamics through time-resolved x-ray diffraction, extended x-ray absorption fine structure (EXAFS), and related x-ray spectroscopies using pump-probe techniques.

The duration of x-ray pulses generated by synchrotrons is determined by the duration of each stored electron bunch, typically >30 ps. Storage of ultrashort bunches of appreciable charge in a ring is problematic because of instabilities arising from bunch-induced wake fields (*10*). However, short electron bunches can exist in a storage ring for a limited time. We demonstrate experimentally that a femtosecond laser pulse can be used to create femtosecond time structure on a long electron bunch through energy modulation of an ultrashort slice of the bunch. Femtosecond synchrotron pulses (with a spectral range extending from infrared to x-ray wavelengths) are then generated from the ultrashort electron slice. As the modulation rapidly dissipates because of the dynamics of electrons within the storage ring, the electron bunch completely recovers between laser interactions. Furthermore, because the modulation is created by a femtosecond optical pulse, there is absolute synchronization between the x-ray probe pulses

[1]Materials Sciences Division, [2]Accelerator and Fusion Research Division, [3]Advanced Light Source, Ernest Orlando Lawrence Berkeley National Laboratory, Berkeley, CA 94720, USA. [4]Applied Science and Technology Graduate Group, University of California Berkeley, Berkeley, CA 94720, USA.

*To whom correspondence should be addressed. E-mail: rwschoenlein@lbl.gov

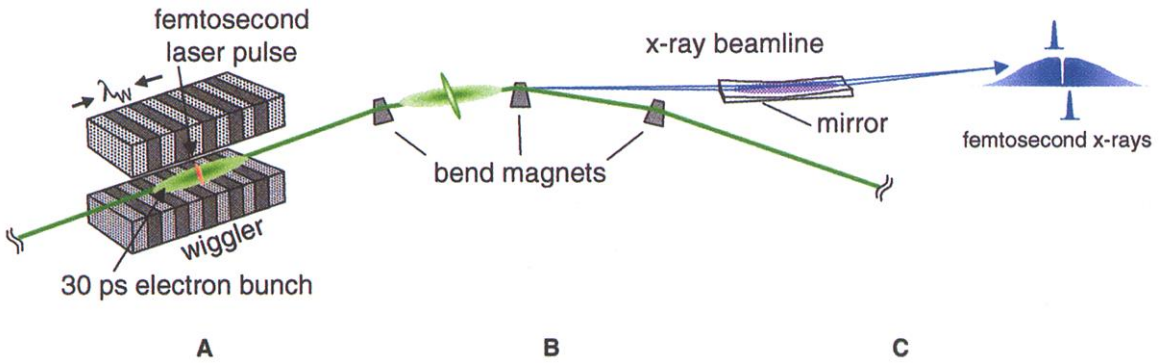

Fig. 1. Schematic of the laser slicing method for generating femtosecond synchrotron pulses. (**A**) Laser interaction with electron bunch in a resonantly tuned wiggler. (**B**) Transverse separation of modulated electrons in dispersive bend of the storage ring. (**C**) Separation of femtosecond synchrotron radiation at the beamline image plane.

and a convenient pump source for triggering dynamic processes.

The bunch modulation is accomplished by co-propagating a femtosecond laser pulse with the stored electron bunch through a wiggler (Fig. 1A). The high electric field of the femtosecond laser pulse ($\sim 10^9$ V m^{-1}) produces an energy modulation in the underlying electrons as they traverse the wiggler (electrons are accelerated or decelerated depending on the optical phase ϕ seen by each electron at the entrance of the wiggler). The optimal interaction occurs when the central wavelength of the spontaneous emission from an electron passing through the wiggler, $\lambda_S = \lambda_W(1 + K^2/2)/2\gamma^2$, satisfies the resonance condition $\lambda_S = \lambda_L$, where λ_L is the laser wavelength, λ_W is the wiggler period, γ is the Lorentz factor, and the deflection parameter $K = eB_o\lambda_W/2\pi mc$ (where B_o is the peak magnetic field of the wiggler, e is the electron charge, m is the electron mass, and c is the speed of light). In addition, the transverse mode of the laser beam must match the transverse mode of the spontaneous radiation from the electron passing through the wiggler, and the laser spectral bandwidth must match the spectrum of the fundamental wiggler radiation averaged over the transverse mode. Under these conditions, the electron energy modulation ΔE is given by (*9*)

$$\Delta E \cong 2\left(A_L A_W \frac{M_W}{\sqrt{2}M_L}\eta_{emit}\right)^{1/2}\cos\phi \quad (1)$$

where A_L is the laser pulse energy, M_W is the number of wiggler periods, M_L is the laser pulse length in optical cycles [measured full width at half maximum (FWHM)], $A_W \cong 4.1\alpha h\nu_L K^2/(2 + K^2)$ is the energy spontaneously radiated by a single electron passing through the wiggler (*11*), α is the fine structure constant, h is Planck's constant, and $\nu_L = c/\lambda_L$. The nonzero electron beam size is accounted for by the coefficient $\eta_{emit} \approx 0.7$ in our case (*12*). We estimate that a 25-fs laser pulse (FWHM of the intensity) with a photon energy of 1.55 eV and a pulse energy $A_L = 100$ μJ will produce an energy modulation amplitude $\Delta E \approx$ 9 MeV with a wiggler of 19 periods.

If the energy modulation of the ultrashort electron slice is several times as large as the electron beam energy spread, then the modulated electrons can be spatially separated from the rest of the electron bunch, in a dispersive bend of the storage ring, by a transverse distance that is several times the horizontal size of the electron beam (Fig. 1B). Finally, by imaging the synchrotron radiation from the displaced electrons to the experimental area, femtosecond x-rays can be separated from the long pulse with an aperture (Fig. 1C). As the electron slice is created through interaction with the laser pulse, the duration of the synchrotron radiation produced by these electrons will be approximately the same as the laser pulse duration. Furthermore, the extraction of an ultrashort slice of electrons leaves behind an ultrashort hole or "dark pulse" in the core of the electron bunch. This dark pulse will appear in the generated x-rays and can also be used for time-resolved spectroscopy.

Our experiments were conducted at the Advanced Light Source (ALS) storage ring operating at $E = 1.5$ GeV [with a root-mean-square (rms) beam energy spread $\sigma_E = 1.2$ MeV (*13*)] using a wiggler with $M_W = 19$ periods, $\lambda_W = 16$ cm, with the gap adjusted to provide a deflection parameter of $K \cong 13$. Femtosecond pulses (laser pulse duration $\tau_L = 100$ fs, $A_L = 400$ μJ, $\lambda_L = 800$ nm, and laser repetition rate $f_L = 1$ kHz) from a Ti:sapphire laser system (*14*) were synchronized to the storage ring master clock with phase-locking techniques (*15*) and directed into the main vacuum chamber to co-propagate with the electron beam through the wiggler. Following the interaction region, a mirror deflects the fundamental spontaneous wiggler emission and the laser beam out of the storage ring to enable direct measurements of the temporal and spectral overlap and the spatial mode matching between the laser pulses and the wiggler radiation.

The efficiency of the interaction between the laser and electron beams was monitored by measuring the gain in the laser pulse energy. This gain is equivalent to the single-pass gain of a free-electron laser and is optimum under the same mode-matching conditions described above. The measured spectral dependence of the laser gain (Fig. 2A, using unamplified pulses from the laser oscillator) as a function of the wiggler emission wavelength (adjusted with the wiggler gap) was compared with the calculated gain based on known parameters of the electron beam (*12, 16*). The agreement between the calculated and measured gain indicates that, under proper conditions, the maximum energy exchange indicated by Eq. 1 can be achieved. Figure 2B shows the gain of the amplified laser

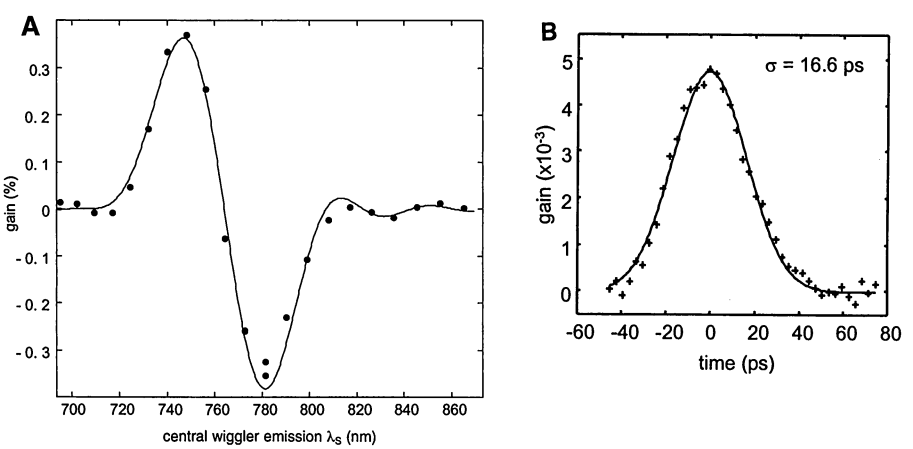

Fig. 2. (**A**) Measured and predicted (solid line) gain in the laser oscillator pulse energy as a function of wiggler tuning λ_S, with $\lambda_L = 780$ nm. (**B**) Measured gain in the amplified laser pulse energy as a function of time delay between the laser pulse and the electron bunch (solid line is a Gaussian fit with $\sigma = 16.6$ ps).

pulses as a function of the relative time position between the laser pulse and the electron bunch. This is an accurate measurement of the electron bunch length and indicates a duration of 39-ps FWHM (at a bunch current of ~3 mA). Typical gain measurements with the amplified beam are ~50% of the expected value, and this is thought to be the result of slight phase-front distortions in the amplified femtosecond laser pulses.

Following interaction with a femtosecond optical pulse in the wiggler, the temporal and spatial evolution of the electron distribution within the bunch was determined by the characteristics of the ALS storage ring lattice. The spatial distribution of the central region of the electron bunch (Fig. 3), following propagation from the interaction region to the bend magnet, was calculated from known lattice parameters (*12*). The time-of-flight properties of the storage ring cause electrons with $\Delta E < 0$ to follow a shorter path and therefore accumulate toward the head of the bunch, whereas electrons with $\Delta E > 0$ follow a longer path and accumulate toward the tail of the bunch. Similarly, the dispersion properties of the ring cause a horizontal displacement ($\Delta x \propto \Delta E$) of the energy-modulated electrons. The horizontal separation of electrons occurs only in particular regions of the storage ring with nonzero dispersion, whereas the temporal separation is cumulative around the ring and gives rise to a stretching of the ultrashort electron slice.

Femtosecond synchrotron radiation pulses are generated from the horizontally displaced electrons, whereas the absence of electrons in the central region of the bunch gives rise to a "dark" femtosecond pulse. The time structure of the temporally incoherent synchrotron radiation is directly determined by the time structure of the electron bunch and is invariant over the entire spectrum of the synchrotron emission, from infrared to x-ray wavelengths. We directly measured the time structure of the visible synchrotron emission using cross-correlation techniques. Visible synchrotron light (~2-eV photon energy) from the beamline was imaged onto a nonlinear optical crystal, along with a delayed 50-fs pulse from the laser system. Photons at the sum frequency were counted as a function of delay between the modulating laser pulse (propagating through the wiggler) and the laser pulse used for cross correlation. An adjustable knife edge located in the beamline at an intermediate image plane provides a means for selecting radiation originating from different transverse regions of the electron beam.

A series of cross-correlation measurements was made at various knife-edge positions, in units of the rms horizontal beam size σ_x (Fig. 4). Measurements of the central core of the synchrotron beam (Fig. 4A) reveal the femtosecond hole or dark pulse that is created because of the acceleration and deceleration of electrons by the laser pulse. The bright pulse is measured with the knife edge at the $3\sigma_x$ position (Fig. 4B) such that the central core of the beam is blocked. Measurements at $4\sigma_x$ (Fig. 4C) reveal a similar femtosecond synchrotron radiation pulse that is shifted slightly later in time, and they demonstrate that the laser pulse provides at least a 6-MeV ($\Delta x = 4\sigma_x$ corresponds to $\Delta E = 5\sigma_E$) energy modulation to a femtosecond slice of the electron bunch.

The solid lines in Fig. 4 are based on the model calculation of the electron bunch distribution shown in Fig. 3. We additionally account for the measured transverse profile of the visible synchrotron light at the image plane, which exhibits non-Gaussian tails beyond $3\sigma_x$, due to the limited collection aperture of the beamline optics. This diffraction of visible wavelengths accounts for the relatively large background levels in the measurements shown in Fig. 4, B and C, but is not an issue at x-ray wavelengths (*17*). At x-ray wavelengths, the dominant contribution to the background is nonspecular scattering from the beamline optics. Such scattering can be minimized so that the integrated flux in a 100-fs x-ray pulse is ~10 times the integrated flux of the 30-ps pulse from which it is extracted (*18*).

A peak energy modulation of $\Delta E = 6.4$ MeV is assumed for the model calculation shown in Fig. 4 and is essentially the only free parameter aside from an amplitude scaling of the signal. The energy modulation is consistent with that predicted by Eq. 1 with the measured laser pulse energy and duration, with an interaction efficiency of ~50%, as indicated by the measured gain. The agreement between the theoretical predictions and the experimental measurements (including the amplitude of the dark pulse, the time shifts of the bright pulses, and the signal-to-background ratios) indicates that the model can be confidently applied to predict the characteristics of the femtosecond x-rays and their dependence on experimental conditions. The location of the bend-magnet beamline used in these demonstration experiments is less than optimum because of the distance from

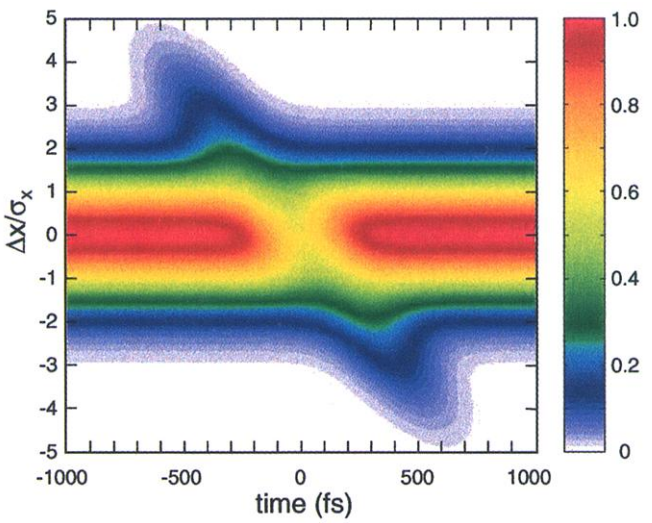

Fig. 3. Model calculation of the electron bunch distribution (as a function of horizontal displacement Δx and time) at the radiating bend magnet, following interaction with the laser pulse in the wiggler, and propagation through 1.5 arc sectors of the storage ring.

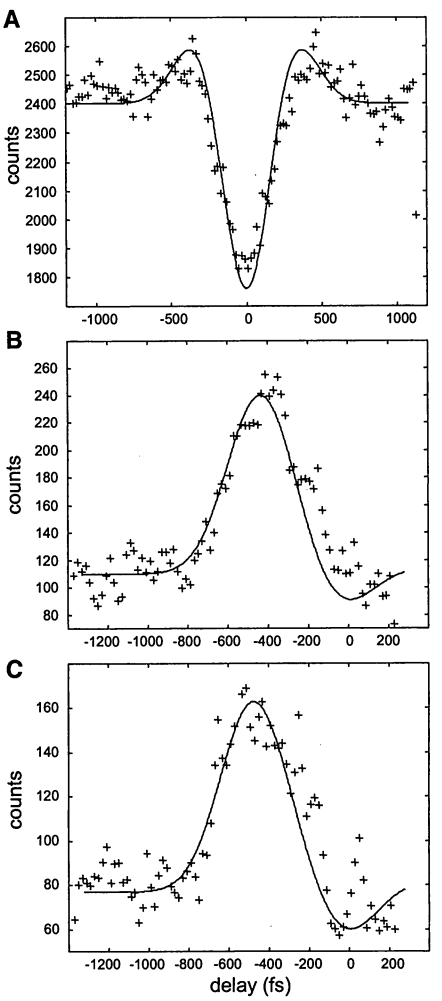

Fig. 4. Cross-correlation measurements of the synchrotron pulse duration for various knife-edge positions: (**A**) radiation collected from $-3\sigma_x$ to $3\sigma_x$, (**B**) radiation collected from $3\sigma_x$ to $8\sigma_x$, and (**C**) radiation collected from $4\sigma_x$ to $8\sigma_x$. Solid lines are from the model calculation shown in Fig. 3.

the wiggler in which the interaction between laser and electron occurs. For a bend magnet located immediately following the wiggler (as shown in Fig. 1), the stretching of the electron distribution due to time-of-flight effects will be reduced by a factor of 3, resulting in an x-ray pulse duration of ~100 fs. In addition, the temporal structure of the electron distribution will give rise to the emission of a single-cycle infrared pulse ($\lambda_o \sim 120$ μm) that is spatially and temporally coherent (*12, 19*).

The average flux and brightness of the femtosecond x-rays can be determined from the full beamline flux and brightness scaled by three factors: $\eta_1 = \tau_L/\tau_e$, $\eta_2 = f_L/f_B$, and $\eta_3 \approx 0.2$, where τ_L and τ_e are the laser pulse and electron bunch durations, respectively; f_L and f_B are the laser and electron bunch repetition rates, respectively; and η_3 accounts for the fraction of electrons that are in the proper phase of the laser pulse to get the maximum energy exchange suitable for creating the large transverse separation. Synchrotron radiation damping provides for recovery of the electron beam between interactions. As the laser interacts sequentially with each bunch, the time interval between interactions is given by N_B/f_L, where N_B is the number of bunches in the storage ring. Furthermore, because the bunch slice is only a small fraction of the total bunch, an interaction interval of ~3 ms [30% of the storage ring damping time (*13*)] is sufficient to allow recovery of the electron beam between laser interactions (*9*). Thus, with 300 bunches in the storage ring, femtosecond x-rays can be generated at repetition rates as high as 100 kHz without adversely affecting the other beamlines at the ALS. On the basis of the known parameters of an ALS bend magnet and undulator at a beam energy of 1.9 GeV (*13, 20*), with $\eta_1\eta_2\eta_3 \approx 10^{-8}$ (for example, laser pulses of 25 fs, 100 μJ at 20 kHz), we expect an average femtosecond flux from a bend magnet of $\sim 10^5$ photons s^{-1} per 0.1% bandwidth (BW) (for a collection angle of 1 mrad) and an average brightness of $\sim 4 \times 10^7$ photons s^{-1} $mrad^{-2}$ mm^{-2} per 0.1% BW at a photon energy of 2 keV. For an ALS small-gap undulator, the average femtosecond flux is $\sim 10^7$ photons s^{-1} per 0.1% BW, and the average brightness is $\sim 10^{11}$ photons s^{-1} $mrad^{-2}$ mm^{-2} per 0.1% BW at a photon energy of 2 keV.

The generation of femtosecond x-rays is an important capability for third-generation synchrotron sources and promises to be a powerful tool for investigating ultrafast structural dynamics in materials. As this approach creates femtosecond time structure on the electron beam, standard radiating devices (bend magnet, wiggler, or undulator) can be designed to emit femtosecond x-ray pulses with the desired properties (bandwidth, tunability, brightness, and so forth). The x-ray flux and brightness levels available from such a femtosecond synchrotron source will enable a wide range of x-ray techniques, including diffraction and EXAFS, to be applied on a 100-fs time scale to investigate atomic motion associated with phase transitions in solids, making and breaking of bonds during chemical reactions, and possibly ultrafast biological processes.

References and Notes

1. T. Elsaesser, J. G. Fujimoto, D. A. Wiersma, W. Zinth, Eds., *Ultrafast Phenomena XI*, vol. 63 of *Springer Series in Chemical Physics* (Springer-Verlag, Berlin, 1998).
2. S. M. Mini, Ed., *Applications of Synchrotron Radiation Techniques to Materials Science IV*, vol. 524 of *Materials Research Society Symposia Proceedings* (Materials Research Society, Warrendale, PA, 1998).
3. A. M. Lindenberg *et al.*, *Phys. Rev. Lett.* **84**, 111 (2000).
4. C. Rischel *et al.*, *Nature* **390**, 490 (1997).
5. C. W. Siders *et al.*, *Science* **286**, 1340 (1999).
6. I. V. Tomov, D. A. Oulianov, P. Chen, P. M. Rentzepis, *J. Phys. Chem. B* **103**, 7081 (1999).
7. R. W. Schoenlein *et al.*, *Science* **274**, 236 (1996).
8. A. H. Chin *et al.*, *Phys. Rev. Lett.* **83**, 336 (1999).
9. A. A. Zholents and M. S. Zolotorev, *Phys. Rev. Lett.* **76**, 912 (1996).
10. C. Limborg, in *Time Structure of X-ray Sources and Its Applications*, A. K. Freund, H. P. Freund, M. R. Howells, Eds., vol. 3451 of *Proceedings of SPIE* (SPIE Press, Bellingham, WA, 1998).
11. D. E. Alferov, Y. A. Bushmakov, K. A. Belovintsev, E. G. Bessonov, P. A. Cherenkov, *Particle Accel.* **9**, 223 (1979).
12. R. W. Schoenlein *et al.*, *Appl. Phys. B*, in press.
13. "1–2 GeV Synchrotron Radiation Source—Conceptual Design Report," *LBL PUB-5172 Rev.* (Lawrence Berkeley Laboratory, Berkeley, CA, 1986).
14. The laser system consists of a Kerr lens mode-locked oscillator, pulse stretcher, multipass amplifier, and pulse compressor. For a review of similar laser systems, see S. Backus, C. G. Durfee, M. M. Murnane, H. C. Kapteyn, *Rev. Sci. Instrum.* **69**, 1207 (1998).
15. M. J. W. Rodwell, D. M. Bloom, K. J. Weingarten, *IEEE J. Quantum Electron.* **25**, 817 (1989).
16. A. Amir and Y. Greenzweig, *Nucl. Instrum. Methods Phys. Res. A* **250**, 404 (1986).
17. For x-rays, the relatively small collection angle of the beamline is more than sufficient to accurately image the source (electron beam) without being limited by diffraction.
18. Measurements of the electron beam profile at the ALS verify that it follows a Gaussian distribution out to $5\sigma_x$, corresponding to a background level of $\sim 10^{-6}$. Measurements of the x-ray beam profile at the image plane of a toroidal imaging mirror demonstrate that the nonspecular scattering in the horizontal plane can be suppressed to $\sim 10^{-4}$ of the peak specular intensity.
19. The field of the coherent single-cycle infrared pulse will correspond exactly to the solid line in Fig. 4A (minus the constant offset), and the flux will scale as the square of the number of absent electrons in the hole or dark pulse.
20. At 1.9 GeV, the average flux from an ALS bend magnet is $\sim 2 \times 10^{13}$ photons s^{-1} per 0.1% BW (for a collection angle of 1 mrad), and the average brightness is $\sim 5 \times 10^{15}$ photons s^{-1} $mrad^{-2}$ mm^{-2} per 0.1% BW at a photon energy of 2 keV. For an ALS small-gap undulator, the average flux is $\sim 10^{15}$ photons s^{-1} per 0.1% BW, and the average brightness is $\sim 10^{19}$ photons s^{-1} $mrad^{-2}$ mm^{-2} per 0.1% BW at a photon energy of 2 keV.

21. This work was supported by the U.S. Department of Energy under contract DE-AC03-76SF00098. The ALS is supported by the Director, Office of Science, Office of Basic Energy Sciences, and Materials Sciences Division of the U.S. Department of Energy under contract DE-AC03-76SF00098 at Lawrence Berkeley National Laboratory. We gratefully acknowledge the use of beamline 6.3.2 and the protein crystallography wiggler (W16) at the ALS and the technical assistance from the ALS Accelerator Physics Group, the ALS Engineering Group, and the ALS operations staff.

17 September 1999; accepted 8 February 2000

A Class of Microstructured Particles Through Colloidal Crystallization

Orlin D. Velev,* Abraham M. Lenhoff, Eric W. Kaler

Microstructured particles were synthesized by growing colloidal crystals in aqueous droplets suspended on fluorinated oil. The droplets template highly ordered and smooth particle assemblies, which diffract light and have remarkable structural stability. The method allows control of particle size and shape from spheres through ellipsoids to toroids by varying the droplet composition. Cocrystallization in colloidal mixtures yields anisotropic particles of organic and inorganic materials that can, for example, be oriented and turned over by magnetic fields. The results open the way to controllable formation of a wide variety of microstructures.

The study of colloidal crystals has provided important fundamental insights into colloidal forces and self-organization (*1, 2*), and the crystals have promise as precursors for advanced materials. Closely packed crystals display a number of potentially usable characteristics such as light diffraction and photonic band gaps (*2–4*), high packing density and surface-to-volume ratio, maximal structural stability, and high catalytic/reactivity throughput. A major barrier to technological application of these structures is the lack of simple, easily controlled methods for mounting or shaping the crystals into usable solid objects.

Here we describe a method to template closely packed colloidal crystals into porous

Center for Molecular and Engineering Thermodynamics, Department of Chemical Engineering, University of Delaware, Newark, DE 19716, USA.

*To whom correspondence should be addressed. E-mail: velev@che.udel.edu